Volume 52
Number 36
28 September 2023
Pages 12567-13012

Dalton Transactions

An international journal of inorganic chemistry

rsc.li/dalton

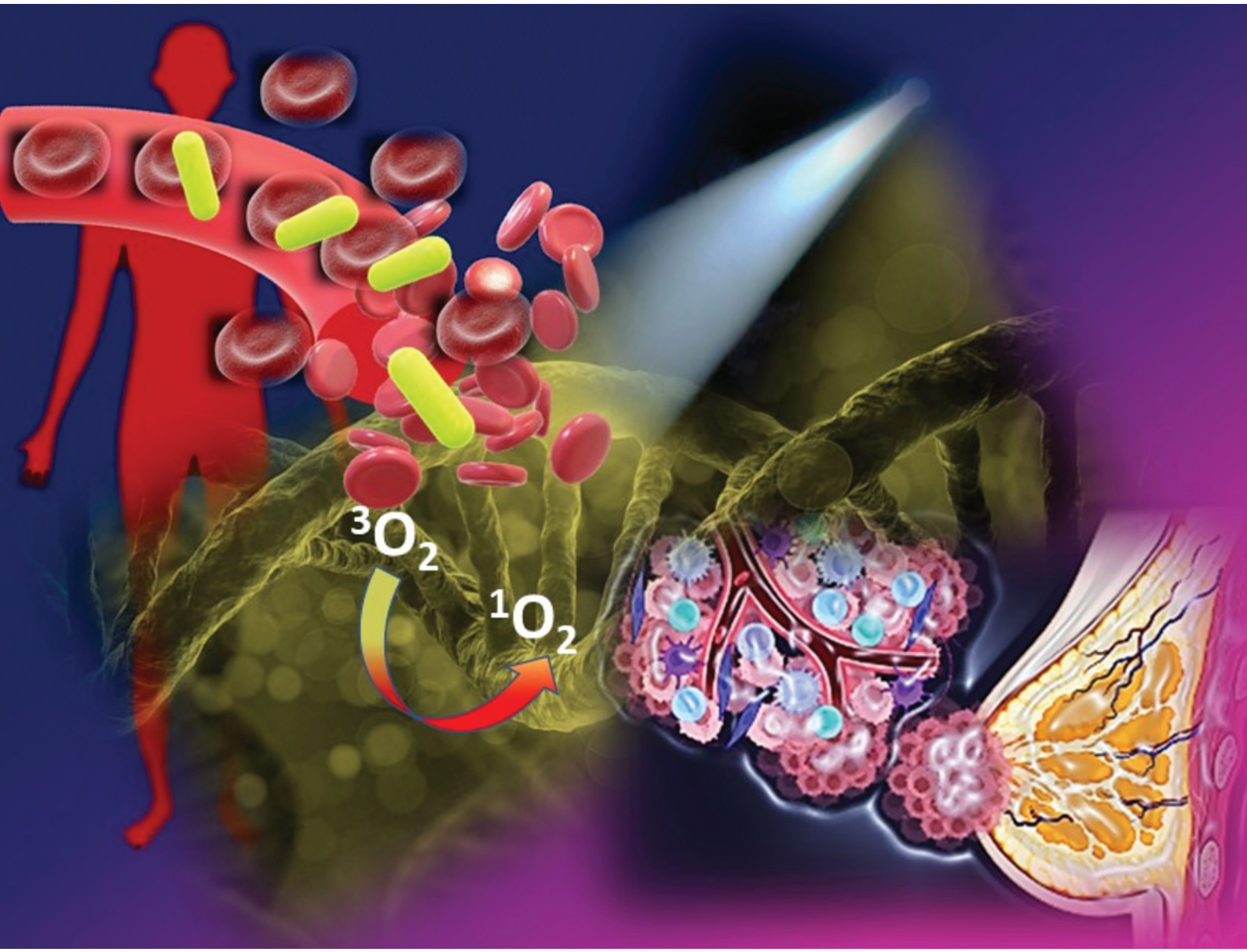

ISSN 1477-9226

ROYAL SOCIETY OF CHEMISTRY

PAPER

Utpal Das and Priyankar Paira
Synthesis, characterization, photophysical and electrochemical properties, and biomolecular interaction of 2,2′-biquinoline based phototoxic Ru(II)/Ir(II) complexes

Dalton Transactions

ROYAL SOCIETY OF CHEMISTRY

PAPER

View Article Online
View Journal | View Issue

Cite this: *Dalton Trans.*, 2023, **52**, 12608

Synthesis, characterization, photophysical and electrochemical properties, and biomolecular interaction of 2,2′-biquinoline based phototoxic Ru(II)/Ir(II) complexes†

Utpal Das and Priyankar Paira *

Received 6th May 2023,
Accepted 26th May 2023

DOI: 10.1039/d3dt01348k

rsc.li/dalton

The phototoxic nature of drugs has been seen to convey immense importance in photo activated chemotherapy (PACT) for the selective treatment of disease. Rationally, in order to eradicate the vehemence of cancer in a living body, the design of phototoxic molecules has been of growing interest in research to establish a selective strategy for cancer therapy. Therefore, the present work portrays the synthesis of a phototoxic anticancer agent by incorporating ruthenium(II) and iridium(III) metals into a biologically active 2,2′-biquinoline moiety, **BQ**. The complexes, **RuBQ** and **IrBQ**, have been revealed as effective anticancer agents with remarkable toxicity in the presence of light compared to the dark towards HeLa and MCF-7 cancer cell lines due to the production of a profuse amount of singlet oxygen ($^1O_2$) upon irradiation by visible light (400–700 nm). Complex **IrBQ** exhibited the best toxicity (IC_{50} = 8.75 μM in MCF-7 and 7.23 μM in HeLa) in comparison to the **RuBQ** complex under visible light. **RuBQ** and **IrBQ** displayed considerable quantum yields (Φ_f) along with a good lipophilic property, indicating the cellular imaging capability of both complexes upon significant accumulation in cancer cells. Also, the complexes have shown significant binding propensity with biomolecules, *viz*. deoxyribonucleic acid (DNA) as well as serum albumin (BSA, HSA).

Introduction

The swift increase in the prevalence of pernicious cancer has become a great peril to the living world, being the second primary cause of death after cardiovascular disease. In the arena of anticancer research, the stupendous discovery of *cis*-diamminedichloroplatinum(II) (cisplatin) by Rosenberg in 1965 paved the way for the exploration of metal complexes as anticancer agents.[1,2] Nonetheless, the ample side effects associated with cisplatin and its congeners because of poor selectivity encouraged researchers to search for appropriate alternatives to platinum-based anticancer metallodrugs.[3] Accordingly after prolonged research, ruthenium and iridium based metallodrugs were seen to be prominent as pertinent alternatives to treat various types of cancer.[4] A plethora of useful properties of iridium(III) and ruthenium(II) complexes, such as high quantum yields, cellular permeability in a high range, a wide range of ligand substitution abilities, large Stokes shifts, low toxicity, potential redox properties, high emission lifetimes, satisfactory photo stability, and stability towards cancer cells, caught the eye for designing the next generation of anticancer drugs.[5] However, selective treatment of cancer along with negligible side effects from drugs, is the main focus of current anticancer research. In this regard, the design of phototoxic molecules offers an opportunity to treat cancer selectively. Like traditional oxygen-dependent photodynamic therapy (PDT), photo-activated chemotherapy (PACT) is another treatment strategy which provides oxygen-independent machinery by a phototoxic molecule. Therefore, photo-activated chemotherapy (PACT) using phototoxic molecules is more appropriate for hypoxic tumors.[6] Ruthenium complexes have been seen to be very active towards selective cancer therapy, overcoming the shortcomings of cisplatin and its congeners.[7] The first Ru(II)-based photosensitizer, TLD1433, was developed for PDT and has undergone human clinical trials.[8] Moreover, studies have also shown that Ru(II) complexes may acquire potential as PACT agents.[9] A. K. Renfrew *et al.* represented a photo-labile ruthenium(II)–purine complex which was capable of releasing 6-mercaptopurine as an anticancer agent upon irradiation by a light beam directed at a tumor.[10] Interestingly, we have successfully synthesized a group of DNA-targeting phototoxic Ru(II)-*p*-cymene dipyridophenazine complexes as phototoxic anticancer agents.[11] C. F. Daher *et al.*

Department of Chemistry, School of Advanced Sciences, Vellore Institute of Technology Vellore-632014, Tamilnadu, India. E-mail: priyankar.paira@vit.ac.in

† Electronic supplementary information (ESI) available. See DOI: https://doi.org/10.1039/d3dt01348k

established the chemotherapeutic potency of a 2,9-diphenyl-1,10-phenanthroline based photoactivable Ru(II) complex, which induced apoptosis in triple-negative MDA-MB-231 breast adenocarcinoma cells.[12] In this connection, B. Elias and co-workers explored the phototoxic behavior of hypoxic active Ir(III)-based anticancer scaffolds towards 3D tumour spheroids.[13] V. Brabec *et al.* synthesised dipyridophenazine-based mitochondria-targeting Ir(III)-complexes which showed phototoxicity against the stem cells of poorly treatable and highly hostile Rhabdomyosarcoma (RD) cells.[14] Moreover, H. Huang *et al.* determined the photocatalytic anticancer profile of an Ir(III) photocatalyst. They demonstrated that these complexes were able to cause photo-induced redox imbalance in cells and changes in mitochondrial membrane potential (MMP), which ultimately led to necrosis as well as apoptosis of cancer cells.[15]

In conjunction with Ru(II) and Ir(III) metals, decorating with bioactive ligands has also gained sound significance on account of their multitargeting properties which can augment the anticancer properties of metal complexes. It has been noticed that heterocycles are the fundamental components of most naturally occurring biologically active compounds. Therefore, these compounds as well as their derivatives have to a great extent been preferred as important pharmacophores for preparing various types of drugs.[16] In this connection, the quinoline moiety has been identified as the key framework in a number of compounds of therapeutic importance.[17,18] Incidentally, the 2,2′-biquinoline (**BQ**) moiety has been chosen as a ligand due to the increased therapeutic response from this molecule as the two quinoline rings are fused together in the vicinity of the N-donor atoms, leaving scope for coordination to metals.[19] Herein, we have introduced 2,2′-biquinoline (**BQ**)-based ruthenium and iridium complexes (**RuBQ** and **IrBQ**) to comprehend their phototoxicity upon clarification of their various chemical and biological properties, which include photophysical behaviour, lipophilicity, stability towards glutathione (GSH) and MTT conditions, electrochemical properties, ROS generation, binding affinity to DNA and serum albumin, and cytotoxicity against MCF-7 and HeLa cancer cell lines.[20] All these salient characteristics of the designed complexes have been depicted in Fig. 1.

Results and discussion

Synthesis and characterization of the complexes

At the outset, the ligand **BQ** was treated with appropriate metal precursors [dichloro(*p*-cymene) ruthenium(II) dimer or dichloro(pentamethylcyclopentadienyl)iridium(III) dimer] and the metal complexes **RuBQ** and **IrBQ** were synthesized with 92%–94% yields (Scheme 1). Using nuclear magnetic resonance (NMR) spectroscopy, IR spectroscopy, and ESI-HRMS (Fig. S1–S12†), we were able to characterize these **RuBQ** and **IrBQ** complexes. The aromatic peaks of *p*-cymene in complex **RuBQ** were observed as two separate doublets in the aromatic region (δ = 5.82 and 6.01 ppm) in the ^{1}H NMR spectrum. The ^{1}H NMR spectrum also showed the expected positions of the typical peaks for –Me protons and –CH protons (δ ~2–3 ppm). In addition to ruthenium isotopic splitting, the distinctive

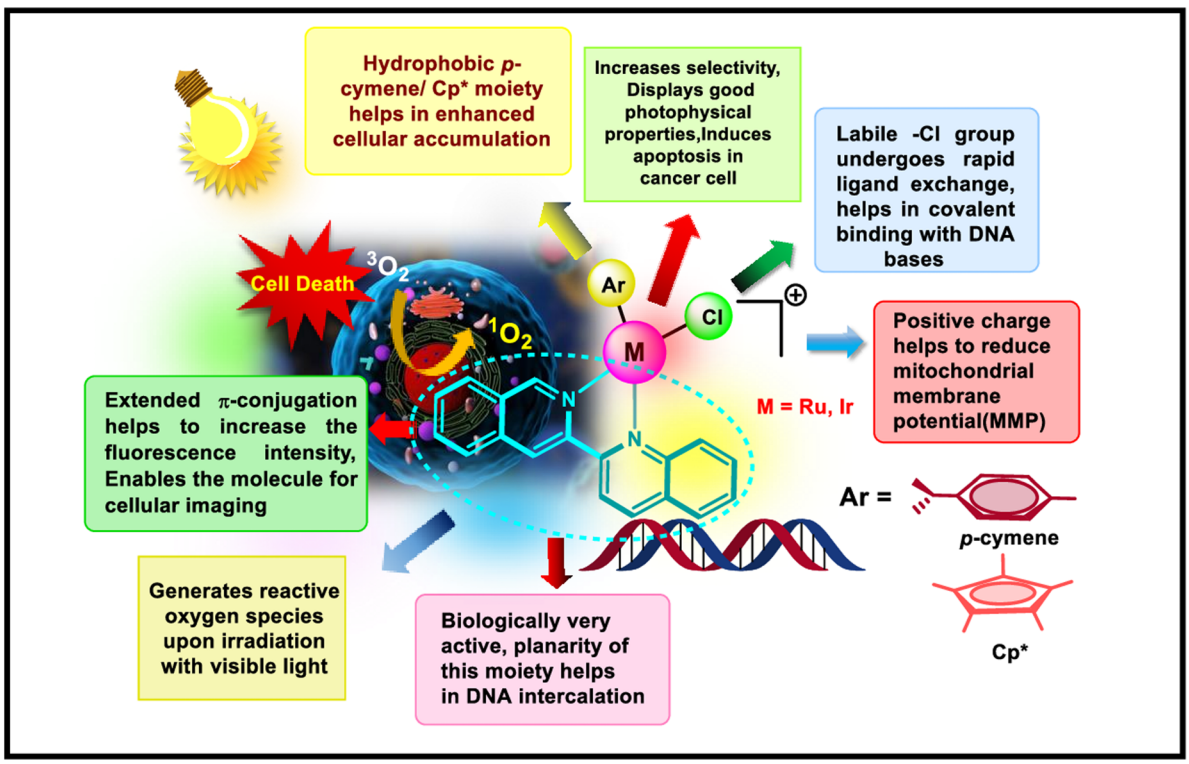

Fig. 1 Design of **RuBQ** and **IrBQ** complexes.

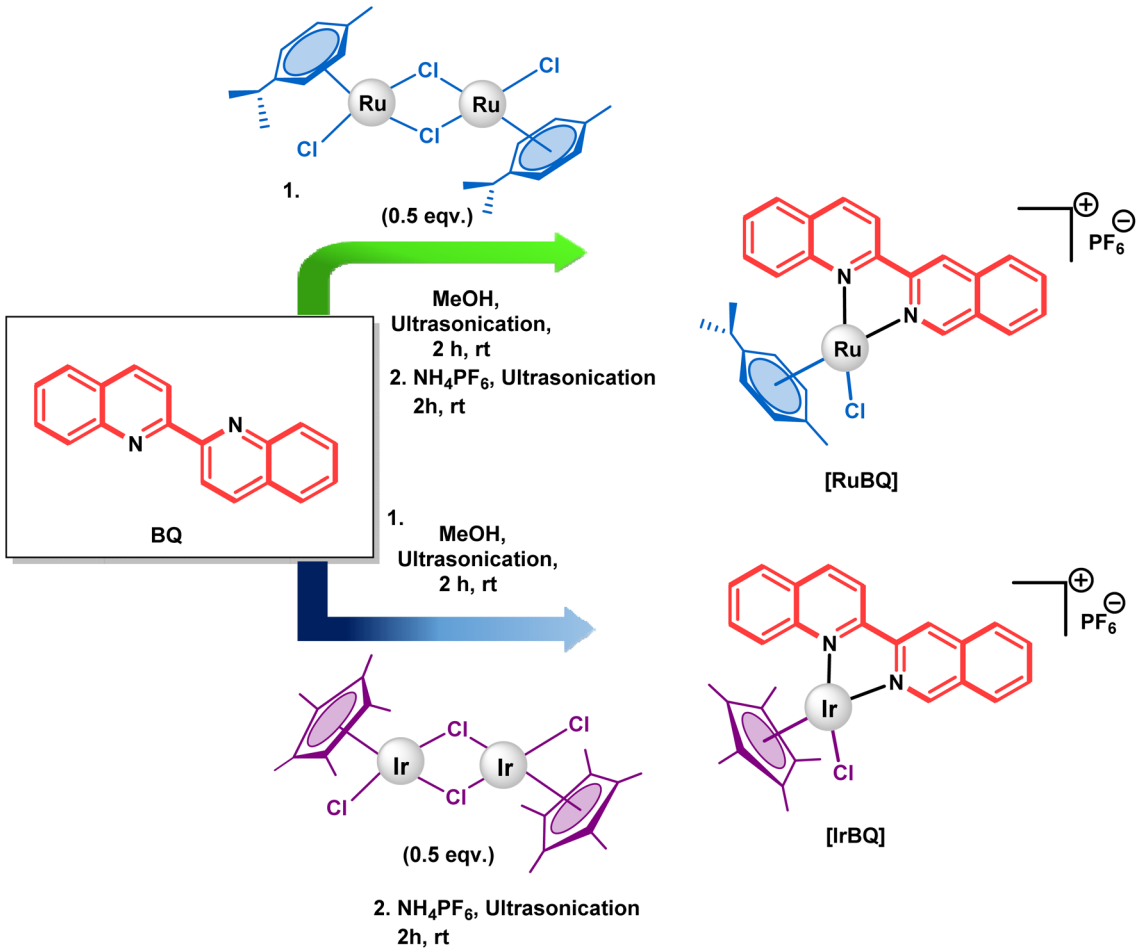

Scheme 1 Synthetic pathways of metal complexes **RuBQ** and **IrBQ**.

molecular ion peak of compound **RuBQ** was seen at 527.0737 $[M - PF_6]^+$. Likewise, the presence of Cp* protons of complex **IrBQ** were observed as a singlet at 1.31 ppm in the ^1H NMR spectrum. The molecular ion peak of complex **IrBQ**, $[M - PF_6]^+$, was detected at 619.1395, which correlated with the literature value. The characteristic carbon peaks of both complexes were also observed in their proper positions in the ^{13}C NMR spectra.

UV-visible and fluorescence study

Absorption spectra were recorded at 298 K for **RuBQ** and **IrBQ** by keeping the concentration at 3×10^{-5} M for both complexes in 10% DMSO–H_2O. Spin-allowed intraligand (ligand to ligand; *i.e.* LLCT) strong absorption bands (π–π^*) were observed in the wavelength range of λ = 260 to 280 nm for both complexes. Also, charge transfer between the metal and the ligand (MLCT) corresponding to the metal-centered HOMO was observed as a broad absorption band in the range of λ = 350 to 400 nm (Fig. S13†). When these complexes were excited at 267 nm they exhibited emission at λ = 335 and 392 nm for **RuBQ** and λ = 329 and 393 nm for **IrBQ** (Fig. S14†). From all these pieces of information, the quantum yield of the complexes was calculated using eqn (i) (see the ESI† for details, Table 1).

Solubility, lipophilicity and conductivity

The ability of metal complexes to prevent tumor growth relies on penetration of the complex through the cell membrane by maintaining a favorable balance between hydrophilicity and lipophilicity. The shake-flask method was used to evaluate the lipophilicity of these complexes.[20] The *n*-octanol/water partition coefficient ($\log P_{o/w}$) values for these metal complexes, **RuBQ** and **IrBQ**, were found to be 0.15 and 0.20, respectively (Table 1). Complex **IrBQ** displayed the highest $\log P_{o/w}$ value (0.20), which could be explained by the fact that the Cp* moiety of iridium metal appears in the most hydrophobic group. The solubility of the metal complexes was examined in a wide variety of solvents. They were decently soluble in 5–10 mg ml^{-1} of DMSO-10% DMEM medium (Dulbecco's Modified Eagle Medium 1 : 99 v/v, which was equivalent to cell media), methanol, acetonitrile, DMF, and ethanol, and were comparatively soluble in water. In DMSO solution, the complexes displayed molar conductivities between 19 and 20 S m^2 mol^{-1}. More importantly, however, it was observed that the

Table 1 Physicochemical characterization of the complexes

	λ_a [a] (nm)								$\wedge_M$ [g] (S m^2 mol^{-1})	
Samples	π–π*	MLCT	λ_f [b] (nm)	Stokes shift	O.D[c]	ε [d] (M^{-1} cm^{-1})	(Φ_f)[e]	log $P_{o/w}$ [f]	DMSO	10% DMSO–H_2O
RuBQ	263	373	335	72	1.28	42333	0.001	0.15	19	62
			392	129						
IrBQ	268	375	329	61	1.83	60666	0.008	0.20	20	68
			393	125						
Quinine sulfate	350	452	102	0.25	8000	0.547	—	—		

[a] Absorption maxima. [b] Emission wavelength. [c] Optical density. [d] Extinction coefficient. [e] Quantum yield. [f] *n*-Octanol/water partition coefficient. [g] Conductance in DMSO and 10% aqueous DMSO.

molar conductivity values increased in 10% DMSO–H_2O medium. The ionization of the Ru–Cl bond, followed by aquation of the complexes, could account for this enhancement.[21]

Stability study of complexes using UV–vis spectroscopy method

The stability of complexes **RuBQ** and **IrBQ** with a concentration of 3×10^{-5} M was evaluated in various media (*i.e.* 1 mM GSH (glutathione), 10% DMSO–PBS (phosphate buffered saline), 1 mM glucose and cysteine) to establish whether they would be effective therapeutic agents in a cancer cell environment. It can clearly be observed in Fig. S15† that **RuBQ** and **IrBQ** were significantly stable in 1 mM GSH (glutathione) medium up to 24 hours, demonstrating that GSH had no such influence on the stability of the metal complexes. A similar effect was also found when we performed the experiment in 10% DMSO–PBS (phosphate buffered saline) medium (Fig. S16†). Glucose was selected as the prospective binding partner for metallodrugs due to its abundance in the bloodstream (the blood glucose level is between 3.6 and 5.8 mM) and hence 1 mM glucose solution was used for this experiment. After recording the data for up to 24 hours, we observed that **RuBQ** and **IrBQ** were effectively stable in 1 mM glucose medium (Fig. S17†). We also performed a similar experiment with 1 mM cysteine (cys) solution and a change in absorbance from 12 to 24 hours was observed, indicating interaction between cys and the metal complex (Fig. S18†).[22,23] We also conducted a stability study with cys, using ^{1}H NMR spectroscopy in DMSO-d_6 (mixed with 1% D_2O). There were two peaks at 2.85 and 3.56 ppm, both of which disappeared after 6 hours of study. This indicated that cys molecules interacted with these complexes in an agreeable way (Fig. S19 and S20†).[22,23]

Electrochemical property

The electrochemical property of these complexes was studied with cyclic voltammetry in order to obtain the stability of the +2 and +3 oxidation states of the ruthenium and iridium complexes. This study was performed in dichloromethane solvent with 2×10^{-3} M concentration at 298 K, using 0.2 M [N-(*n*-Bu)$_4$] PF_6 as the supporting electrolyte with the scan rate fixed at 100 mV s^{-1}. Both complexes were found to exhibit a type of irreversible electrochemical behavior. We inferred the redox potential of the synthesized complexes to be iridium(III)/iridium(II), ruthenium(III)/ruthenium(II) based on the obtained electrode potential values (Fig. 2).[24]

DNA binding study

UV–visible method. DNA is the primary pharmacological target for many anticancer drugs, and the binding pattern of the anticancer scaffolds depends on how they interact with DNA. The UV–visible spectroscopic technique was used to determine the binding constant (K_b) and type of interaction. Base pairs of DNA, pyrimidines (cytosine and thymine) and purines (adenine and guanine), are seen to provoke electronic transitions. The λ_{max} were observed to be 257 nm and 268 nm for **RuBQ** and **IrBQ**, respectively, with a concentration of 5×10^{-5} M, and the corresponding absorbance intensity exhibited hypochromism with an increase in DNA concentration (Fig. S21† and Table 2). Owing to the hypochromic shift, we can conclude that the intercalative mode of binding is feasible between the metal complex and DNA. The intrinsic binding constants (K_b) were found to be 0.20×10^5 M^{-1} and 0.25×10^5 M^{-1} for complexes **RuBQ** and **IrBQ**, respectively (Fig. S21,† Table 2, eqn (ii) (see the ESI† for details)). Sequence specificity verification was confirmed by selecting adenine and guanine as two base pairs. This study was performed by fixing the concentration of both complexes at 20 μM and varying the adenine and guanine concentrations from 0 to 35 μM. Based on these findings, we inferred that the complexes bind to the base pair through a hyperchromic effect (Fig. S22 and S23†). This suggested the possibility of major and minor groove binding.[25,26]

Ethidium bromide displacement assay. The intercalation of the synthesized complexes to ct-DNA was further proved by an EtBr displacement assay recorded in a spectrofluorometer. At first, EtBr did not show any kind of fluorescence property, but after the addition of EtBr to ct-DNA, a significant fluorescence intensity was observed at λ_{ems} = 595 nm upon excitation at λ_{abs} = 485 nm due to the formation of a DNA–EtBr adduct through intercalation of EtBr into the DNA base pair. However, the fluorescence intensity gradually decreased (hypochromic nature) with successive increases in the concentration of the metal complexes (Fig. S24†). This indicated that EtBr was removed from the DNA–EtBr adduct as the intercalative interaction happened progressively between DNA and the metal complexes.

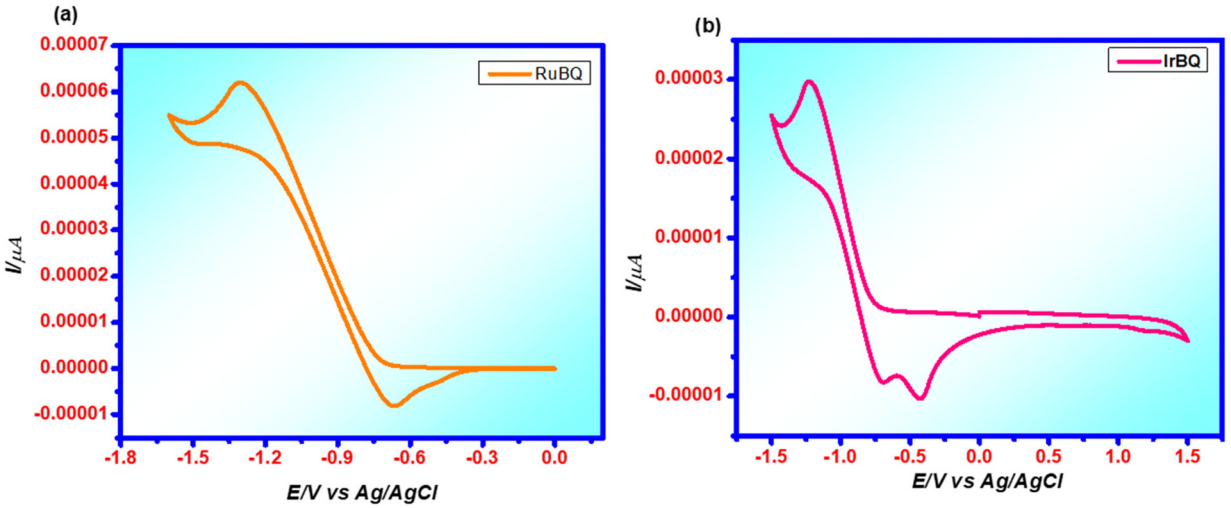

Fig. 2 CV of synthesized complexes in DCM solvent at 298 K. Conditions: 0.2 M [N-(n-Bu)$_4$]PF$_6$ supporting electrolyte, scan rate 100 mV s^{-1}.

Table 2 Binding parameters for the interaction of all the complexes with ct-DNA

Complex	λ_{max} [nm]	Change in absorbance intensity	K_b [a] ($\times 10^5$ M^{-1})	K_{SV} [b] ($\times 10^6$ M^{-1})	K_{app} [c] ($\times 10^6$ M^{-1})
RuBQ	257	Hypochromism	0.20	0.129	2.0
IrBQ	268	Hypochromism	0.25	0.205	2.28

[a] K_b, intrinsic DNA binding constant from UV–vis absorption titration. [b] K_{SV}, Stern–Volmer quenching constant. [c] K_{app}, apparent DNA binding constant from competitive displacement.

With the help of eqn (iii) (see the ESI† for details) we found the K_{app} values to be 2×10^6 M^{-1} and 2.28×10^6 M^{-1} for complexes **RuBQ** and **IrBQ**, respectively (Table 2, eqn (iii)). The K_{sv} values were found to be 0.129×10^6 M^{-1} and 0.205×10^6 M^{-1} for complexes **RuBQ** and **IrBQ**, respectively (Table 2, eqn (iv), see the ESI† for details).[20,25]

Viscosity measurement. The effects of the relative specific viscosity by addition of the complexes in ct-DNA solutions were investigated with the help of an Ostwald viscometer following a hydrodynamic method. Upon the addition of a metal complex to a ct-DNA solution, the specific viscosity increased, as predicted for intercalative binding. This observation suggested elongation of the ct-DNA double helix, which was connected to base-pair separation through the adaptation of complexes into ct-DNA base pairs. The metal complexes might twist the DNA double helix through non-classical binding, which would affect the optimal length and viscosity of the DNA. Also, groove binding and electrostatic binding might be possible for metal complexes by interacting with the terminal site of DNA strands through van der Waals or hydrophobic interactions. Here, with the help of the eqn $(\eta/\eta_0)^{1/3} = 1 + \beta R$, we plotted $(\eta/\eta_0)^{1/3}$ *vs.* $1/R$, where R = [DNA base pairs]/[metal complex], $(\eta/\eta_0)^{1/3}$ = the relative specific viscosity of ct-DNA, and η and η_0 are the specific viscosity of DNA in the presence and absence of the metal complex. The viscosity of both complexes was determined in the presence of ct-DNA with respect to EtBr. Intercalative binding between the metal complexes and ct-DNA along with some extent of electrostatic or groove binding was suggested to be possible by the fact that a slight increase in viscosity was discerned when the complexes were added to ct-DNA solution (Fig. S25†).[5]

BSA binding study

Serum albumin is a key plasma protein involved in the uptake, transport and metabolism of a wide range of exogenous and endogenous elements pertaining to metabolic processes within cells. By means of fluorescence spectroscopy, we analyzed the binding capacity of metal complexes **RuBQ** and **IrBQ** with bovine serum albumin (BSA). A significant fluorescence intensity at 342 nm was observed for the BSA molecule upon excitation at 295 nm (Fig. S26†). As the concentration of metal complexes was gradually increased, the fluorescence intensity of BSA started to decrease noticeably (as depicted by the plot). K_q and K_{BSA} were then estimated using the Stern–Volmer eqn (v) (see the ESI† for details). K_{BSA} values of the **RuBQ** and **IrBQ** complexes were calculated as 0.1822×10^6 M^{-1} and 0.200×10^6 M^{-1}, respectively, whereas the K_q values were found to be 1.822×10^{13} M^{-1} s^{-1} and 2.00×10^{13} M^{-1} s^{-1} (Table 3). The higher value of K_q compared to the value of BSA's maximal

Table 3 Binding parameters for the interaction of both complexes with BSA

Complex	K_{BSA} [a] [$\times 10^6$ M^{-1}]	K_q [b] [$\times 10^{13}$ M^{-1} s^{-1}]	K [c] [$\times 10^4$ M^{-1}]	n [d]
RuBQ	0.182	1.822	1.88	1.47
IrBQ	0.200	2.000	3.90	1.34

[a] K_{BSA}, Stern–Volmer quenching constant. [b] K_q, quenching rate constant. [c] K, binding constant with BSA. [d] n, number of binding sites.

scatter collision quenching constant (2.0×10^{10} M^{-1} s^{-1}) suggested a static quenching linkage seemed to have taken place. By using the Scatchard eqn (vi) (see the ESI† for details), not only were we able to determine the total number of binding sites (n) in these complexes, but we were also able to determine their overall binding constants (K) (Table 3). These complexes are assumed to be highly effective in treating cancer cells because of their strong interaction with serum albumin, which overrides GSH-mediated drug resistance.[5,20,23,27]

HSA binding study

To correlate the BSA binding behavior of these complexes with human serum albumin (HSA), a fluorescence-based binding experiment was also performed with HSA. HSA, a protein abundant in the environment surrounding a human cell, facilitates drug entry into the cell by forming a more active coordinate complex. Significant fluorescence at 333 nm was observed for the HSA molecule upon excitation at 280 nm (Fig. S27†). With a gradual increase in the concentration of the metal complexes, the fluorescence intensity of HSA was found to decrease, as depicted by the plot. K_q and K_{HSA} were estimated using the Stern–Volmer eqn (v) (see the ESI† for details). The K_{HSA} values of complexes **RuBQ** and **IrBQ** were observed as 0.3070×10^6 M^{-1} and 0.1624×10^6 M^{-1} and K_q values as 3.070×10^{13} M^{-1} s^{-1} and 1.624×10^{13} M^{-1} s^{-1}, respectively (Table 4). Similarly, the K_q values were found to be greater than the maximum value of the dynamic quenching constant (2.0×10^{10} mol^{-1} s^{-1}), which also confirmed the possibility of static quenching, effective bimolecular quenching, and bimolecular binding with these molecules. Using the Scatchard eqn (vi) (see the ESI† for details), we were able to determine the total number of binding sites for these complexes and their binding constants (Table 4).[5,20,25,27]

Singlet oxygen generation ($^1O_2$)

By performing a 1,3-diphenylisobenzofuran (DPBF) test with the help of a UV–vis spectrophotometer, we determined how well the complexes could facilitate photo-sensitized singlet oxygen generation. We employed Rose Bengal (RB) as a typical singlet oxygen generator and the highly reactive diene DPBF as a fluorescent probe in this investigation. Singlet oxygen ($^1O_2$) interacted with DPBF at room temperature to form an endoperoxide, which was then quickly broken down into 1,2-dibenzoylbenzene. A substantial decrease in the absorbance of DPBF was observed at 417 nm in the presence of the complexes (Fig. 3) which was an indication of the photoactivated production of singlet oxygen by the complexes that could be quantified with respect to a standard like Rose Bengal (Fig. 3). Therefore, it can be depicted that the absorbance of DPBF at 417 nm gradually diminished in a time-dependent way after exposure to visible light (400–700 nm, 10 J cm^{-2}) in the presence of the complexes. We plotted the relative changes in absorbance of DPBF treated with Rose Bengal and then treated with complexes at 417 nm (A/A_0) with time (s) (where A_0 = the absorbance of DPBF at t = 0 s and A = the absorbance of DPBF at a specific time). A linear reduction in absorbance of DPBF with time indicated the photo-induced synthesis of $^1O_2$ from $^3O_2$ *via* a type-II photochemical process. The singlet oxygen quantum yields were found to be 0.047 and 0.052 for complexes **RuBQ** and **IrBQ**, respectively (eqn (vii) and (viii)) and the results were comparable to the singlet oxygen quantum yield (ϕ) of Rose Bengal (standard) of 0.76. It is worth mentioning that no change in absorbance of DPBF was visualized in the presence of either complex or Rose Bengal when we performed the experiment in dark conditions.[28–30]

Table 4 Binding parameters for the interaction of both complexes with HSA

Complex	K_{HSA} [a] [$\times 10^6$ M^{-1}]	K_q [b] [$\times 10^{13}$ M^{-1} s^{-1}]	K [c] [$\times 10^4$ M^{-1}]	n [d]
RuBQ	0.307	3.070	2.132	1.41
IrBQ	0.162	1.624	2.298	1.50

[a] K_{HSA}, Stern–Volmer quenching constant. [b] K_q, quenching rate constant. [c] K, binding constant with HSA. [d] n, number of binding sites.

In vitro cytotoxicity study

The *in vitro* cytotoxicity of both complexes **RuBQ** and **IrBQ** in comparison to the control drug, cisplatin, were evaluated *via* the typical 3-(4,5-dimethylthiazol-2-yl)-2,5-diphenyltetrazolium bromide (MTT) assay protocol beside a panel of cancer cell lines, *i.e.* human epithelioid cervical carcinoma (HeLa), and human breast cancer cell line (MCF-7), in triplicate. The cells were exposed to yellow light (0–2 J cm^{-2}) from a 400 W tungsten lamp fitted with a heat isolation filter and 500 nm long pass filter at an intensity of 4 mW cm^{-2} for 4 hours in the presence of both complexes. However, both complexes conveyed insignificant dark toxicity against both cancer cell lines (IC_{50} ~ 20 μM). These complexes exhibited significant cytotoxic behaviour (IC_{50} ~ 7–10 μM, PI > 2) in the presence of yellow light compared to dark conditions. Between the Ru(II) and Ir(III) complexes, **IrBQ** showed the highest potency against both cell lines (IC_{50} in MCF-7 = 8.75 ± 0.46 μM and in HeLa cells = 7.23 ± 0.79 μM) (Table 5). However, both complexes exhibited higher potency and selectivity than cisplatin under both dark and light conditions. Again, the potency of complexes **RuBQ** and **IrBQ** has been justified with reference to some reported examples of Ru and Ir based PACT agents along with their properties which have been nicely represented in a table (Fig. S28 and Table S1†).[11,31–37,38–43] Thereby, these complexes may provide a useful scaffold in cancer therapy in the presence of light, presiding over the prevailing anticancer drug, cisplatin.

Experimental section

Materials and methods

All of the reagents and solvents used in the experiment were of the highest possible quality and purity levels available for commercial use. There was no further purification of the organic solvents employed in the chemical synthesis and chromato-

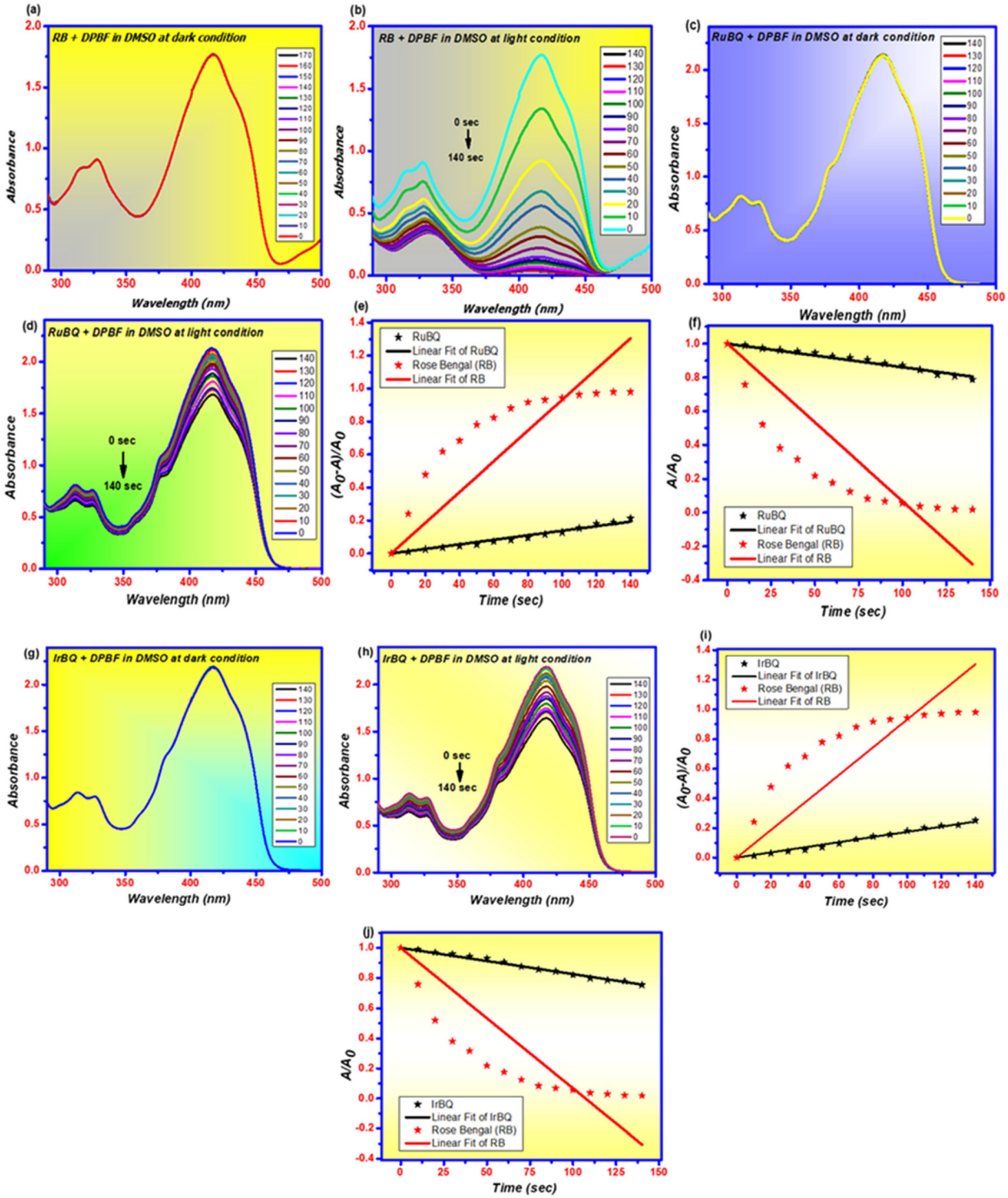

Fig. 3 UV–visible spectroscopic analysis for the creation of singlet oxygen by adding Rose Bengal [(a) dark conditions, (b) in the presence of light], by adding complex **RuBQ** [(c) dark conditions, (d) in the presence of light] and adding complex **IrBQ** [(g) dark conditions, (h) in the presence of light] in a solution of DPBF at 298 K. (e) Competitive singlet oxygen generation plot in between RB and complex **RuBQ** $(A_0 - A)/A_0$ *vs.* time (s) and (i) complex **IrBQ**. (f) Relative changes in the absorbance of DPBF in the case of both Rose Bengal and complexes, **RuBQ** (A/A_0) with time and (j) complex **IrBQ** at 417 nm.

graphy because they were of analytical grade. Products such as dichloro-(pentamethylcyclopentadienyl) iridium(III)dimer, dichloro(*p*-cymene) ruthenium(II) dimer, ammonium hexafluorophosphate, 2,2′-biquinoline, deoxyribonucleic acid sodium salt (DNA), bovine serum albumin (BSA), and L-glutathione reduced (GSH) were purchased from reputable

Table 5 Light and dark toxicity of complexes **RuBQ** and **IrBQ**[11]

	IC_{50} [a] (μM)					
	MCF-7[b]			HeLa[c]		
Complex	Dark	In light	PI[d]	Dark	In light	PI
RuBQ	20.12 ± 0.64	9.45 ± 0.58	2.12	24.12 ± 0.62	10.48 ± 0.76	2.30
IrBQ	19.19 ± 0.43	8.75 ± 0.46	2.19	17.15 ± 1.46	7.23 ± 0.79	2.37
Cisplatin	9.42 ± 0.66	9.10 ± 0.54	1.03	15.6 ± 0.54	14.26 ± 0.48	1.09

[a] IC_{50}: 50% of cells experience cell death. [b] Human breast cancer cell line. [c] Human epithelioid cervical carcinoma cancer cell lines. [d] PI: phototoxicity index.

suppliers like Sigma-Aldrich Chemicals Limited, Spectrochem, and E-Merck, respectively. All of the NMR spectra were recorded on a high-powered Bruker DPX spectrometer using tetramethyl silane (TMS) as a standard. Experiments on viscosity were performed with an Ostwald viscometer, and the conductivity of the complexes was measured with a TDS conductometer-307. Infrared (IR) spectra of the complexes were recorded using a Shimadzu Affinity FT-IR spectrometer throughout the range 4000–400 cm^{-1}. For the UV–visible experiment, we utilized a JASCO V-730 spectrophotometer equipped with a 1 cm quartz cell, and for the fluorescence experiment, we used a Hitachi F7000 fluorescence spectrophotometer equipped with a xenon lamp.

Synthesis and characterization of the complexes

Synthetic technique of RuBQ. 25 mg of ligand **BQ** (1 equiv) and 30 mg of $[Ru^{II}_2(\eta^6\text{-}p\text{cym})_2(Cl)_4]$ (0.5 equiv) were utilized to synthesize **RuBQ**, as described in earlier work.[25] A brown coloured complex was formed.

Yield: 94%; color: brown; Mp: 197–200 °C; R_f (pure methanol): 0.56. ^{1}H NMR (DMSO-d_6, 400 MHz): δ 9.02 (dd, 4H, J = 8.8 Hz, ArH), 8.94 (d, 2H, J = 8.8 Hz, ArH), 8.30 (d, 2H, J = 8.0 Hz, ArH), 8.15–8.11 (t, 2H, J = 8.0 Hz, ArH), 7.98–7.95 (t, 2H, J = 7.6 Hz, ArH), 6.01 (d, 2H, J = 6.0 Hz, *p*-cymene ArH), 5.82 (d, 2H, J = 6.0 Hz, *p*-cymene ArH), 2.32 (s, 3H, *p*-cymene aliphatic methyl proton), 1.94–2.01 (m, 1H, *p*-cymene aliphatic –CH proton), 0.75 (d, 6H, J = 8.0 Hz, *p*-cymene isopropyl methyl proton); ^{13}C NMR (DMSO-d_6, 100 MHz): δ 156.98, 149.81, 141.83, 133.36, 130.34, 129.87, 129.66, 129.57, 120.91, 104.43, 86.77, 86.43, 30.49, 21.87, 18.34; ^{19}F NMR (DMSO-d_6, 376 MHz): δ −71.04 (PF_6), −69.16 (PF_6); ^{31}P NMR (DMSO-d_6, 162 MHz): δ −153.02 to −135.46 (PF_6); HRMS (MeOH): m/z = 527.0737 $[M - PF_6]^+$.

Synthetic technique of IrBQ. 19 mg of ligand **BQ** (1 equiv) and 30 mg of $[Ir^{III}_2(\eta^5\text{-}cp^*)_2(Cl)_4]$ (0.5 equiv) were utilized to synthesize **IrBQ**, as described in earlier work.[15] A reddish-brown coloured complex was formed.

Yield: 92%; color: reddish-brown; Mp: 270–272 °C; R_f (pure methanol): 0.51. ^{1}H NMR (DMSO-d_6, 400 MHz): δ 9.01 (s, 4H, ArH), 8.63 (d, 2H, J = 8.8 Hz, ArH), 8.31 (d, 2H, J = 8.0 Hz, ArH), 8.14–8.10 (t, 2H, J = 8.0 Hz, ArH), 7.98–7.95 (t, 2H, J = 7.2 Hz, ArH), 1.31 (s, 15H, *Cp** protons); ^{13}C NMR (DMSO-d_6, 100 MHz): δ 157.68, 146.42, 142.84, 133.68, 130.49, 130.28, 129.88, 129.39, 121.17, 90.05, 8.90; ^{19}F NMR (DMSO-d_6, 376 MHz): δ −71.04 (PF_6), −69.16 (PF_6); ^{31}P NMR (DMSO-d_6, 162 MHz): δ −153.02 to −135.46 (PF_6); HRMS (MeOH): m/z = 619.1395 $[M - PF_6]^+$.

Conclusions

Briefly, it can be said that we have successfully synthesized and characterized a pair of visible-light-stimulated phototoxic anticancer agents, **RuBQ** and **IrBQ**. Specific study of these two complexes has shown that both complexes are significantly toxic towards MCF-7 and HeLa cancer cell lines upon irradiation with visible light in comparison to dark conditions. The cancer cell toxicity of **RuBQ** and **IrBQ** can be attributed to their good binding propensity with DNA bases and ability to release singlet oxygen species to destroy cancer cells. These complexes have shown strong binding efficacy with serum albumin (BSA, HSA) present in blood plasma, indicating their good transportation through the bloodstream after being administered to the body. It has been noticed that both molecules have attained a capability to penetrate the cellular membrane with ease because of their substantial lipophilicity. Therefore, it can be depicted that these two phototoxic complexes will be eligible for selective cancer therapy under visible light after being usefully delivered to the cancer cells.

Conflicts of interest

There are no conflicts to declare.

Acknowledgements

The authors are grateful to VIT for 'VIT SEED GRANT'. We acknowledge DST, New Delhi, India for the DST-FIST project. Authors are grateful to the Department of Science and Technology, Government of India for supporting the work through the DST-SERB CRG project grant (CRG/2021/002267).

References

1 B. Rosenberg, L. V. Camp, E. B. Grimley and A. J. Thomson, The inhibition of growth or cell division in Escherichia coli by different ionic species of platinum(IV) complexes, *J. Biol. Chem.*, 1967, **242**, 1347–1352.
2 S. Dasari and P. B. Tchounwou, Cisplatin in cancer therapy: molecular mechanisms of action, *Eur. J. Pharmacol.*, 2014, **740**, 364–378.
3 U. Ndagi, N. Mhlongo and M. E. Soliman, Metal complexes in cancer therapy – an update from drug design perspective, *Drug Des., Dev. Ther.*, 2017, **11**, 599–616.

4 (*a*) M. Frik, A. Martínez, B. T. Elie, O. Gonzalo, D. Ramírez de Mingo, M. Sanaú, R. Sánchez-Delgado, T. Sadhukha, S. Prabha, J. W. Ramos, I. Marzo and M. Contel, In vitro and in vivo evaluation of water-soluble iminophosphorane ruthenium(II) compounds. A potential chemotherapeutic agent for triple negative breast cancer, *J. Med. Chem.*, 2014, **57**, 9995–10012; (*b*) P. Steunenberg, A. Ruggi, N. S. van den Berg, T. Buckle, J. Kuil, F. W. B. van Leeuwen and A. H. Velders, Phosphorescence Imaging of Living Cells with Amino Acid-Functionalized Tris(2-phenylpyridine) iridium(III) Complexes, *Inorg. Chem.*, 2012, **51**, 2105–2114.

5 (*a*) N. Roy, U. Sen, Y. Madaan, V. Muthukumar, S. Varddhan, S. K. Sahoo, D. Panda, B. Bose and P. Paira, Mitochondria-Targeting Click-Derived Pyridinyltriazolylmethylquinoxaline-Based Y-Shaped Binuclear Luminescent Ruthenium(II) and Iridium(III) Complexes as Cancer Theranostic Agents, *Inorg. Chem.*, 2020, **59**, 17689–17711; (*b*) Z. Liu, I. Romero-Canelón, A. Habtemariam, G. J. Clarkson and P. J. Sadler, Potent Half-Sandwich Iridium(III) Anticancer Complexes Containing C^N-Chelated and Pyridine Ligands, *Organometallics*, 2014, **33**, 5324–5333; (*c*) L. He, Y. Li, C. P. Tan, R. R. Ye, M. H. Chen, J. J. Cao, L. N. Ji and Z. W. Mao, Cyclometalated iridium(III) complexes as lysosome-targeted photodynamic anticancer and real-time tracking agent, *Chem. Sci.*, 2015, **6**, 5409–5418.

6 K. L. Eales, K. E. R. Hollinshead and D. A. Tennant, Hypoxia and metabolic adaptation of cancer cells, *Oncogenesis*, 2016, **5**, 190.

7 S. Y. Lee, C. Y. Kim and T-G. Nam, Ruthenium Complexes as Anticancer Agents: A Brief History and Perspectives, *Drug Des., Dev. Ther.*, 2020, **14**, 5375–5392.

8 S. Monro, K. L. Colón, H. Yin, J. Roque, P. Konda, S. Gujar, R. P. Thummel, L. Lilge, C. G. Gameron and S. A. McFarland, Transition Metal Complexes and Photodynamic Therapy from a Tumor-Centered Approach: Challenges, Opportunities, and Highlights from the Development of TLD1433, *Chem. Rev.*, 2019, **119**, 797–828.

9 C. Mari, V. Pierroz, S. Ferrari and G. Gasser, Combination of Ru (II) complexes and light: New frontiers in cancer therapy, *Chem. Sci.*, 2015, **6**, 2660–2686.

10 H. Chan, J. B. Ghrayche, J. Wei and A. K. Renfrew, *Eur. J. Inorg. Chem.*, 2017, **2017**, 1537.

11 B. Kar and P. Paira, One pot three component synthesis of DNA targeting phototoxic Ru(ii)-*p*-cymene dipyrido[3,2-*a*:2′,3′-*c*]phenazine analogues, *Dalton Trans.*, 2022, **51**, 15686–15695.

12 N. Mansour, K. Bodman-Smith, R. S. Khnayzer and C. F. Daher, A photoactivatable Ru (II) complex bearing 2,9-diphenyl-1,10-phenanthroline: A potent chemotherapeutic drug inducing apoptosis in triple negative human breast adenocarcinoma cells, *Chem.-Biol. Interact.*, 2021, **336**, 109317.

13 R. Bevernaegie, B. Doix, E. Bastien, A. Diman, A. Decottignies, O. Feron and B. Elias, Exploring the phototoxicity of hypoxic active iridium(III)-based sensitizers in 3D tumor spheroids, *J. Am. Chem. Soc.*, 2019, **141**, 18486–18491.

14 L. Markova, V. Novohradsky, J. Kasparkova, J. Ruiz and V. Brabec, Dipyridophenazine iridium(III) complex as a phototoxic cancer stem cell selective, mitochondria targeting agent, *Chem.-Biol. Interact.*, 2022, **360**, 109955.

15 C. Huang, C. Liang, T. Sadhukhan, S. Banerjee, Z. Fan, T. Li, Z. Zhu, P. Zhang, K. Raghavachari and H. Huang, *In vitro* and *In vivo* Photocatalytic Cancer Therapy with Biocompatible Iridium(III) Photocatalysts, *Angew. Chem., Int. Ed.*, 2021, **60**, 9474–9479.

16 J. Iqbal, S. A. Ejaz, I. Khan, E. Ausekle, M. Miliutina and P. Langer, Exploration of quinolone and quinoline derivatives as potential anticancer agents, *J. Pharm. Sci.*, 2019, **27**, 613–626.

17 M. F. A. Mohamed and G. E-D. A. Abuo-Rahma, Molecular targets and anticancer activity of quinoline–chalcone hybrids: literature review, *RSC Adv.*, 2020, **10**, 31139.

18 H-W. Huang, Y-D. Bow, C-Y. Wang, Y-C. Chen, P-R. Fu, K-F. Chang, T-W. Wang, C-H. Tseng, Y-L. Chen and C-C. Chiu, DFIQ, a Novel Quinoline Derivative, Shows Anticancer Potential by Inducing Apoptosis and Autophagy in NSCLC Cell and In Vivo Zebrafish Xenograft Models, *Cancers*, 2020, **12**, 1348.

19 M. Kubanik, H. Holtkamp, T. Söhnel, S. M. F. Jamieson and C. G. Hartinger, Impact of the Halogen Substitution Pattern on the Biological Activity of Organoruthenium 8-Hydroxyquinoline Anticancer Agents, *Organometallics*, 2015, **34**, 5658–5668.

20 B. Kar, U. Das, S. De, S. Pete, A. Sharma S, N. Roy, A. K. SK, D. Panda and P. Paira, GSH-resistant and highly cytoselective ruthenium(II)-p-cymene-(imidazo[4,5-f,][1,10]phenanthrolin-2-yl)phenol complexes as potential anticancer agents, *Dalton Trans.*, 2021, **50**, 10369–10373.

21 (*a*) T. A. Khan, K. Bhar, R. Thirumoorthi, T. K. Roy and A. K. Sharma, Design, synthesis, characterization and evaluation of the anticancer activity of water-soluble half-sandwich ruthenium(II) arene halido complexes, *New J. Chem.*, 2020, **44**, 239–257; (*b*) L. T. Babu and P. Paira, 9-Arylacenaphtho[1,2-*b*]quinoxalines *via* Suzuki coupling reaction as cancer therapeutic and cellular imaging agents, *New J. Chem.*, 2021, **45**, 20447–20458; (*c*) I. Ali, W. A. Wani and K. Saleem, Empirical Formulae to Molecular Structures of Metal Complexes by Molar Conductance, *Synth. React. Inorg., Met.-Org., Nano-Met. Chem.*, 2013, **43**, 1162–1170.

22 N. M. Giles, A. B. Watts, G. I. Giles, F. H. Fry, J. A. Littlechild and C. Jacob, Metal and Redox Modulation of Cysteine Protein Function, *Chem. Biol.*, 2003, **10**, 677–693.

23 M. Lukács, D. C. Pálinkás, G. Szunyog and K. Várnagy, Metal Binding Ability of Small Peptides Containing Cysteine Residues, *Chem. – Eur. J.*, 2021, **10**, 451–463.

24 (*a*) K. Purkait and A. Mukherjee, Cytotoxicity and reactivity of a redox active 1,4-quinone-pyrazole compound and its Ru(II)-p-cymene complex, *Inorg. Chim. Acta*, 2020, **502**, 119361; (*b*) T. R. Steel, K. K. H. Tong, T. Söhnel,

S. M. F. Jamieson, L. J. Wright, J. D. Crowley, M. Hanif and C. G. Hartinger, Homodinuclear organometallics of ditopic N,N-chelates: Synthesis, reactivity and in vitro anticancer activity, *Inorg. Chim. Acta*, 2021, **518**, 120220.

25 U. Das, S. Shanavas, A. H. Nagendra, B. Kar, N. Roy, S. Vardhan, S. K. Sahoo, D. Panda, B. Bose and P. Paira, Luminescent 11-{Naphthalen-1-yl} dipyrido [3, 2-a: 2′, 3′-c] phenazine-Based Ru (II)/Ir (III)/Re (I) Complexes for HCT-116 Colorectal Cancer Stem Cell Therapy, *ACS Appl. Bio Mater.*, 2023, **6**, 410–424.

26 J. G. Goll and H. Holden Thorp, Oxidation of DNA by *trans*-dioxoruthenium(VI) complexes: self-inhibition of DNA cleavage by metal complexes, *Inorg. Chim. Acta*, 1996, **242**, 219–223.

27 L. E. H. Paul, B. Therrien and J. Furrer, Interactions of Arene Ruthenium Metallaprisms with Human Proteins, *Org. Biomol. Chem.*, 2012, **51**, 1057–1067.

28 A. Bhattacharyya, A. Dixit, S. Banerjee, B. Roy, A. Kumar, A. A. Karande and A. R. Chakravarty, BODIPY appended copper(II) complexes for cellular imaging and singlet oxygen mediated anticancer activity in visible light, *RSC Adv.*, 2016, **6**, 104474–104482.

29 N. Gandra, A. T. Frank, O. Le Gendre, N. Sawwan, D. Aebisher, J. F. Liebman, K. N. Houk, A. Greer and R. Gao, Possible singlet oxygen generation from the photolysis of indigo dyes in methanol, DMSO, water, and ionic liquid, 1-butyl-3-methylimidazolium tetrafluoroborate, *Tetrahedron*, 2006, **62**, 10771–10776.

30 M. Hoebeke and X. Damoiseau, Determination of the singlet oxygen quantum yield of bacteriochlorin*a*: a comparative study in phosphate buffer and aqueous dispersion of dimiristoyl-l-α-phosphatidylcholine liposomes, *Photochem. Photobiol. Sci.*, 2002, **1**, 283–287.

31 J. Yang, Q. Cao, W. L. Hu, R. R. Ye, L. He, L. N. Ji, P. Z. Qin and Z. W. Mao, *Dalton Trans.*, 2017, **46**, 445–454.

32 S. Roy, E. Colombo, R. Vinck, C. Mari, R. Rubbiani, M. Patra and G. Gasser, *ChemBioChem*, 2020, **21**, 2966–2973.

33 J. Chen, Q. Tao, J. Wu, M. Wang, Z. Su, Y. Qian, T. Yu, Y. Wang, X. Xue and H. K. Liu, *J. Inorg. Biochem.*, 2020, **210**, 111132.

34 N. Tian, Y. Feng, W. Sun, J. Lu, S. Lu, Y. Yao, C. Li, X. Wang and Q. Zhou, *Dalton Trans.*, 2019, **48**, 6492–6500.

35 R. Boerhan, W. Sun, N. Tian, Y. Wang, J. Lu, C. Li, X. Cheng, X. Wang and Q. Zhou, *Dalton Trans.*, 2019, **48**, 12177–12185.

36 P. Srivastava, M. Verma, A. Kumar, P. Srivastava, R. Mishra, S. Sivakumar and A. K. Patra, *Dalton Trans.*, 2021, **50**, 3629–3640.

37 R. P. Paitandi, V. Sharma, V. D. Singh, B. K. Dwivedi, S. M. Mobin and D. S. Pandey, *Dalton Trans.*, 2018, **47**, 17500–17514.

38 Y. Zheng, L. He, D. Y. Zhang, C. P. Tan, L. N. Ji and Z. W. Mao, *Dalton Trans.*, 2017, **46**, 11395–11407.

39 X. D. Song, B. B. Chen, S. F. He, N. L. Pan, J. X. Liao, J. X. Chen, G. H. Wang and J. Sun, *Eur. J. Med. Chem.*, 2019, **179**, 26–37.

40 J. Liu, C. Jin, B. Yuan, X. Liu, Y. Chen, L. Ji and H. Chao, *Chem. Commun.*, 2017, **53**, 2052–2055.

41 M. Ouyang, L. Zeng, K. Qiu, Y. Chen, L. Ji and H. Chao, *Eur. J. Inorg. Chem.*, 2017, **2017**, 1764–1771.

42 X. D. Bi, R. Yang, Y. C. Zhou, D. Chen, G. K. Li, Y. X. Guo, M. F. Wang, D. Liu and F. Gao, *Inorg. Chem.*, 2020, **59**, 14920–14931.

43 R. R. Ye, C. P. Tan, L. He, M. H. Chen, L. N. Ji and Z. W. Mao, *Chem. Commun.*, 2014, **50**, 10945–10948.